

Rotation effects on the Lyman- α line morphology in distant galaxies

Nicolas Garavito-Camargo¹, Jaime E. Forero-Romero¹

¹*Departamento de Física, Universidad de los Andes, Cra. 1 No. 18A-10, Edificio Ip, Bogotá, Colombia*

31 May 2013

ABSTRACT

Rotation is present in the gas kinematics of galaxies up to the highest redshifts. In this paper we present for the first time radiative transfer calculations that show the impact of rotation on the morphology of the Lyman α line. To this end we construct simplified models where a galaxy is modeled as an homogeneous sphere composed as an homogeneous mixture of dust and hydrogen at a constant temperature. These spheres have a solid-body rotation with linear velocities at the surface in the range $0 - 300 \text{ km s}^{-1}$. We consider radiation sources both in the center of the rotating cloud and also homogeneously distributed around the sphere. We find that higher rotational velocities increase the width of each peak in the outgoing line profile while it also increases the amount of Lyman alpha photons escaping in the line center. This trends makes that for high rotational velocities and large Hydrogen optical depths the double peak of the line tends to be erased and be replaced by a single peak the lines center. This is more pronounced for radiation sources homogeneously distributed. Concerning the escape fraction we find that rotation does not have any effect, provided that all the sources are centrally emitted. However in the case of homogeneously emitted sources we measure an increase of about a factor of 2 in the escape fraction for higher rotational velocity values. Our work shows clearly that gas rotation has a non negligible impact on the shape of the Lyman α line.

Key words: galaxies: high-redshift - galaxies: star formation - line: formation

1 INTRODUCTION

Due to the resonant nature of the Lyman alpha line, gas kinematics play an important role shaping its morphology. In the literature there has been extensive studies of out-flow/inflow configurations.

In this paper we study for the first time the impact of rotation on the morphology of the Lyman α line. To isolate the effects of rotation we focus on a simple system: the gas distribution is spherical, with homogeneous density and the gas rotates as a solid body. We base our work on the Monte Carlo base radiative transfer code CLARA (?).

This paper is structured as follows.

2 IMPLEMENTATION OF BULK GAS ROTATION

We implement into CLARA the simplest model whereby a sphere rotates with homogeneous angular velocity. We define a cartesian coordinate system with its origin at the center of the sphere and the rotation axis to be the z -axis, the

components in the bulk velocity field, $\vec{v} = v_x \hat{i} + v_y \hat{j} + v_z \hat{k}$, in the gas can be written as

$$v_x = -\frac{y}{R} V_{\max}, \quad (1a)$$

$$v_y = \frac{x}{R} V_{\max}, \quad (1b)$$

$$v_z = 0, \quad (1c)$$

where R is the radius of the sphere and V_{\max} is the linear velocity at the sphere's surface. The minus sign in the x -component of the velocity indicates the direction of rotation, in this case we assume that the angular velocity vector goes in the \hat{k} direction. The linear dependence of the velocity on the radial distance describes the case of constant angular velocity $\omega = V_{\max}/R$.

We take the polar angle θ that a unitary vector makes with the rotation axis as defined by the dot product $\cos \theta = \hat{u} \cdot \hat{k}$. In the Section 4 we will present in detail how the line differs at different observing angles θ .

Velocity (km s^{-1})	V_{max}	0, 50, 100, 200, 300
Hydrogen Optical Depth	τ_H	$10^5, 10^6, 10^7$
Dust Optical Depth	τ_A	0,1
Photons Distributions		Central, Homogeneous

Table 1. Values for the varying input parameters in CLARA. Taking into account all the possible combinations for these models

3 GRID OF SIMULATED MODELS

We compute the emergent Lyman- α line for several models with different values for the maximal rotational velocity, hydrogen optical depth, dust optical depth and initial distributions of the photons with respect to the gas. There are in total 60 models with the input parameters summarized in Table 1.

4 RESULTS

The central result of this paper is summarized in Fig. 1 where we show that rotation has a considerable effect on the morphology of the emergent Lyman-alpha line both in the case where the photons are emitted at the sphere's center and when they are initialized with an homogeneous distribution all over the gas volume.

The results for these outgoing spectra are integrated over the whole sphere, meaning that all the escaping photons were taking into account regardless of the direction of the outgoing photons. Fig. 2 shows how if one gives a weight to each outgoing photon according to its direction when escaping the gas distribution it is possible to detect notable differences in the spectrum for different viewing angles.

In the following subsections we quantify the trends observed in Fig. 1 and Fig. 2 as a function of the maximum rotation velocity V_{max} and the position of the observer with respect to the rotation angle, $\mu = \cos \theta$. All the results in this section will be expressed in terms of rest frame wavelength.

First we quantify the line by its full width at half maximum (FWHM) and the peak positions. In order to interpret these results we measure how the rotation affects the average number of scatterings for each Lyman-alpha photon in the simulation. This helps us to introduce the next subsection on the escape fraction in our models including dust. We conclude the section by estimating the expected line flux for top hat filters at a fixed center and varying width.

4.1 Line width and peak maxima

The first quantitative conclusion of the effect of rotation in the Lyman alpha line is that the double peaks in the line tend to broaden until they reach a single broad emission peak. This is most evident in the case of Lyman-alpha sources homogeneously distributed in the gas distributions (Fig. 1 Right panel).

To quantify the line broadening we measure a modified version of the full width at half maximum (FWHM) for half of the line, $W_{1/2}$. It means that in the case of double peaked emission, $W_{1/2}$ corresponds to the width of one of the peaks, while in the extreme case when the line is converted into a single peak, $W_{1/2}$ corresponds to half of the full width.

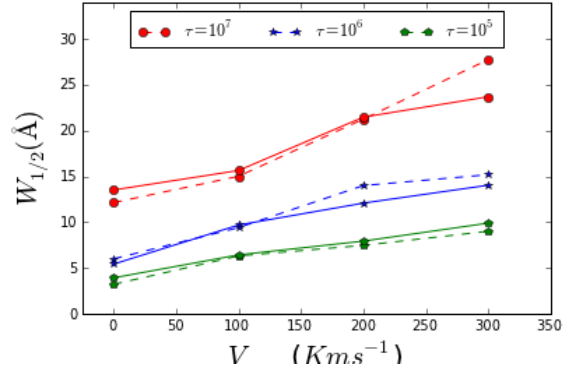


Figure 3. Width of the lyman-alpha line for all the models.

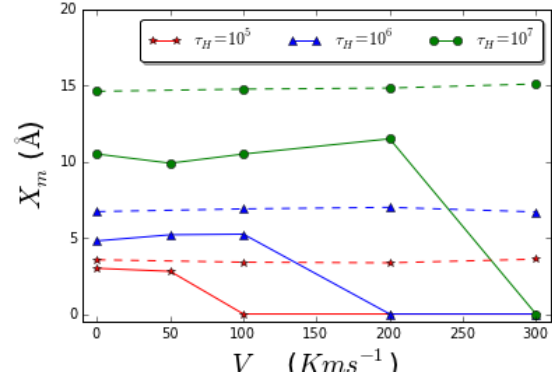


Figure 4. Position of the maxima in the outgoing spectra for different Rotational velocities, (up) Central Distribution, (Down) Homogeneous Distribution.

This definition allows us to quantify the line width both in the cases of double and single peak emission. Furthermore it has the advantage that this line width should have a direct observational correspondence to the observed line feature once the Inter-Galactic Medium (IGM) effects are taken into account, which have the central effect of strongly reducing the intensity of the blue peak of the line.

Fig. 3 summarizes our findings for $W_{1/2}$ as a function of V_{max} . The line width increases with the rotational velocity of the gas cloud. This increase can be of a factor of 2 – 3 with respect to the width with respect to the static case. This trend is conserved at all optical depths regardless of the initial source distribution.

This result includes all the outgoing photons, regardless of the position of the observer. In Figure ?? we take into account the different positions of the observer in the measurement of the half-width $W_{1/2}$. From this we conclude that observers with a line of sight perpendicular to the axis of rotation (i.e. edge-on in the case of spiral galaxy) tend to measure larger line widths than observers aligned with the rotation axis (i.e. face-on). The influence of the observer position on the line width, amounting always less than 15% of a difference with respect to the result that takes into account all the outgoing photons with the same weight regardless of the relative observer position.

The second feature in the line that we use to quantify

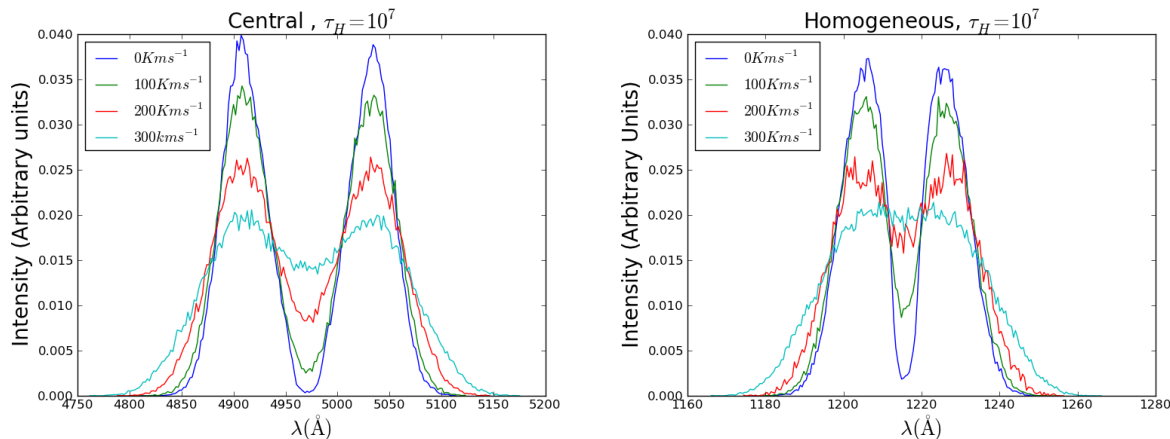


Figure 1. Shape of the Lyman alpha line for different velocities. The left (right) panel shows the central (homogeneous) photon distribution. All photons were taken into account regardless of their outgoing direction of propagation.

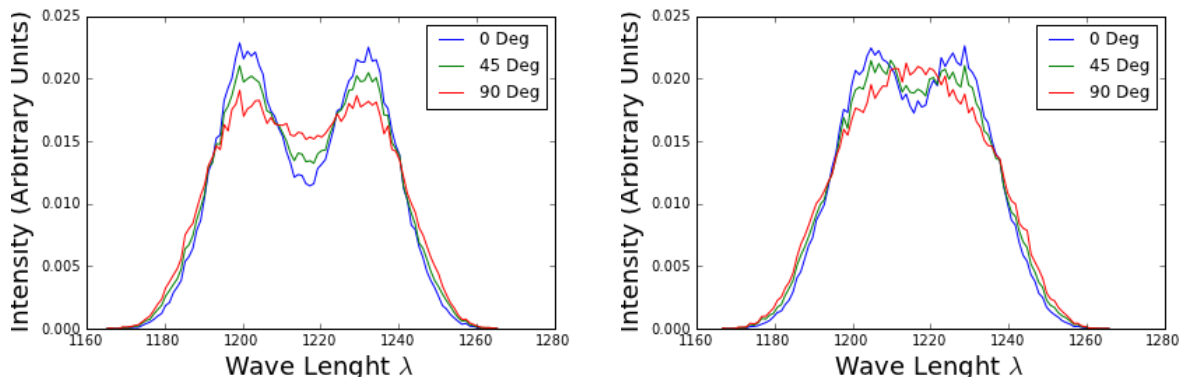


Figure 2. Same as Figure 1 but this time the different lines show the line morphology for different polar angles θ with respect to the rotation axis. In this case each photon has a weight dependent on their outgoing direction. All spectra correspond to the same $V_{\max} = 300 \text{ km s}^{-1}$, Optical Depth $\tau = 10^7$ and Central Distribution without dust.

the effect of rotation is the position of the line maxima. These provide information on the wavelength of the majority of the outgoing photons after they interact with the neutral hydrogen atoms in the gas cloud. If most of the photon escapes with a low number of scattering, its outgoing frequency will be close to its initial frequency, that is in the center of the line. On the contrary if the number of scatterings is large for the average photon, its outgoing frequency will be far from the line center. Such reasoning can be made more quantitative to understand the dependence of the peak maxima as a function of the hydrogen optical depth in the cloud [citation needed].

In Fig. 4 we present the position of the maxima as a function of V_{\max} . For the photons emitted in the line center we do not find any variation in the position of the maxima in the range of explored parameter space (dash lines). However in the homogeneous case we can see how the maxima goes to $x_m = 0$, meaning that the double peak is converted into a single peak.

This transition to a single peak line occurs for the systems where it becomes easier for a bulk of the photons to escape with the lowest number of scatterings possible. This can explain how the single peak stage can be achieved in

the homogeneous source distribution where there is fraction of the photons inside a photosphere region with $\tau_H \sim 1$ which allows them to escape within one scatter. Increasing the rotational velocity makes it easier for the photons in this photosphere region to escape.

We also take into account the viewing angle μ for all the optical depths and rotational velocities and the two different photon distribution. But we don't find any dependency meaning that the peaks would be placed in the same place no matter the position of an external observer.

Finally we also report on the effect of the neutral Hydrogen optical depth τ_H on the maxima position x_m Fig. 4. We find that, at fixed rotation velocity, the position of the maxima increases with optical depth as expected from basic theoretical considerations. We compare our results with the expected theoretical scaling for an infinite slab.

4.2 Average Number of Scatterings

Until now we have focus in how rotation affect the morphology of the Lyman alpha line, now we turn to study deeply the possible causes of this effects. As recombination is the main cause of the emission of the Lyman alpha line, it

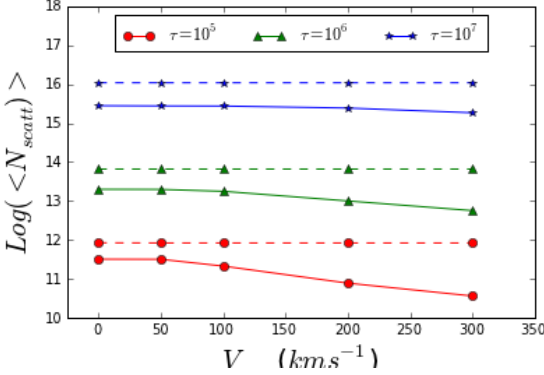


Figure 5. Log of the Average number of scatterings of the outgoing photons as function of the velocity.

is important to study the relationship between the number of times that a photon is absorbed and re emitted that we simply take as scatterings with it's shift in the wavelength.

As a first approach we study the number of scatterings of all the photons at different velocities and for both photon distributions Figure 5. For the central distribution we found that the average number of scattering does not have a relevant change ($\sim 0.5\%$) with V_{max} , For the Homogeneous distribution we found that as V_{max} increase the average number of scatterings decrease in $\sim 39\%$, it means that rotation makes photons to escape easier from the cloud. The reason why this is not observed in the central distribution is because the amount of gas that every photon has to break through is so large that the average number of scatterings is large too, making the effect of rotation unobservable.

In order to understand the effects of rotation in the morphology of the line we make histograms of $\langle N_{scatt} \rangle$ in function of X_m for both the central Fig. 6 and the homogeneous distribution Fig. 7. For the central distribution and for lower velocities we found that for some value (put the value) of N_{scatt} the majority of photons have a defined value of X_m . While for higher velocities photons tend spread out in X_m (Make position analysis of this photons).

For the homogeneous distribution we found the same effect but also, for highest velocities the majority of the photons near the surface escape with much less scatterings that in the static case. This analysis let us conclude that rotation make photons escape with less scatterings and it spread out the wavelength of the of the outgoing photons represented by X_m .

4.3 Escape Fraction

Until now we have studied models in absence of dust, but is known (REFERENCE) that there is presence of dust in high redshift galaxies. Our models with dust are treated as is explained in detail in the appendix of (Forero et al 2011).

Of particular interest is to compute the escape fraction of Lyman α photons coming from the most distant galaxies, due to the fact that with the observed intensity of the Lyman alpha line quantities as the LF and SFR can be derived (put some references).

Previous studies have shown the correlation of the Escape fraction with galactic mass (Laursen et al 2009, Dayal

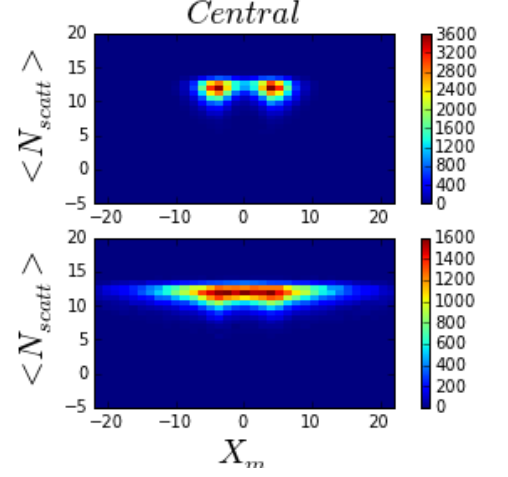


Figure 6. Histogram of N_{scatt} vs X_m for the central distribution, The upper plot is for $V_{max} = 50 \text{ km/s}$, the bottom plot is for $V_{max} = 300 \text{ km/s}$

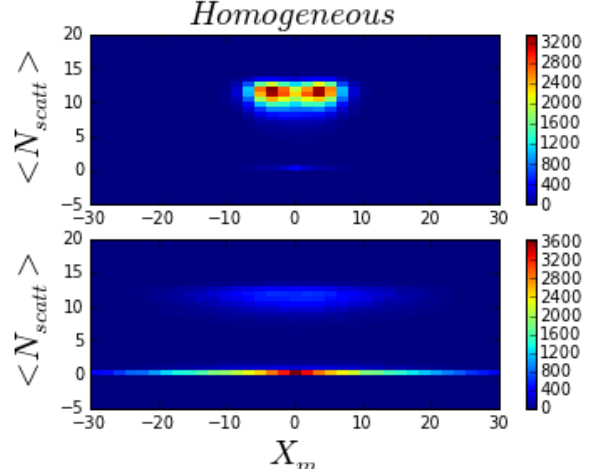


Figure 7. Histogram of N_{scatt} vs X_m for the homogeneous distribution, The upper plot is for $V_{max} = 50 \text{ km/s}$, the bottom plot is for $V_{max} = 300 \text{ km/s}$

et al 2010) abundances and the kinematics of dust. In order to study pure rotational effects in the escape fraction we fixed the dust abundance $\tau_A = 0.01$ and the galaxy mass. We compute the escape fraction for the models described in Table 1.

For a realistic model we also take into account the viewing angle, first we fixed the viewing angle at $\theta = 0$ Fig. 8 and then we fixed the velocity in order to see the escape fraction correlation with the viewing angle. Therefore we define the escape fraction as:

$$F_e = \frac{\Sigma_{NI} \vec{k} \cdot \vec{o}}{\Sigma_{NF} \vec{k} \cdot \vec{o}} \quad (2)$$

Where NI is the initial number of photons and NF is the final, \vec{k} is the rotation axis direction and \vec{o} the observer direction. With this definition we compute the escape fraction for all of our models, the results are presented in

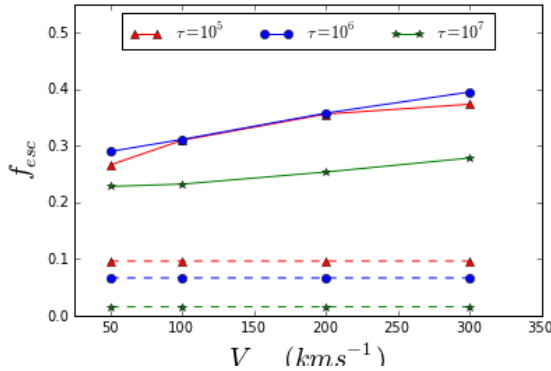


Figure 8. Escape fraction for all the models. continuous lines represent the homogenous models, while dashed lines represent the central models

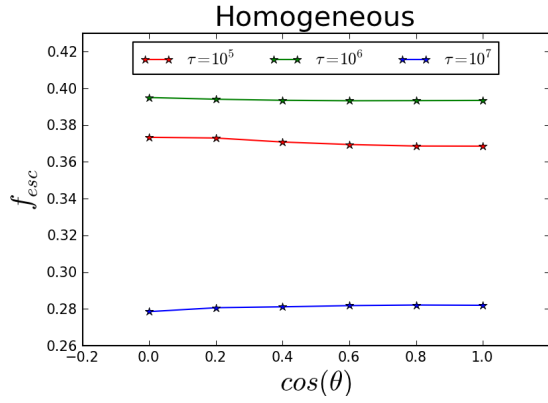


Figure 9. Escape fraction dependency with the viewing angle in the homogeneous configuration.

Fig 8

In Figure 8 we found that in the central distribution the escape fraction does not change with velocity while it does in the optical depth (See Verhamme 2006, an argument about this). On the other hand for the homogeneous distribution we found that for higher velocities photons escape easily. The difference between this two results rely in the fact that in the homogeneous distribution photons are emitted closer to the escape surface and this makes this configuration more sensitive to rotation while in the central configuration the escape fraction depends mainly in the amount of gas rather than in rotation.

As a final test we compare our results with the analytical solution of the slab developed by (Neufeld 1990) Fig. 4.5, as the geometry we use is different from the one described for Neufeld, we don't expect the same results, in fact we found that for the homogenous sphere the escape fraction is higher than the slab (see ref, mark). Also we note that for $\tau < 10^6$ the escape fraction does not increase as it will be expected, This is due to the fact that the condition $a\tau_h \gg \tau_d$ is not valid any more.

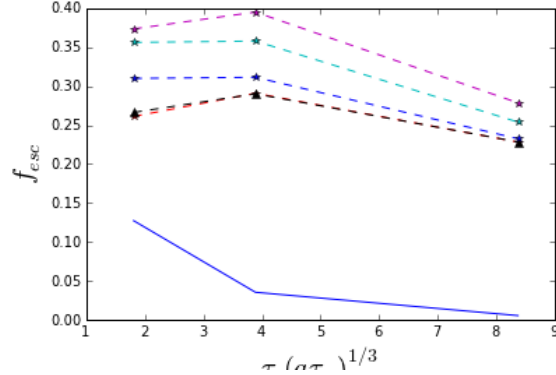


Figure 10. Escape fraction of this work compared with Neufeld analytical solution

4.4 Inhomogeneous model

Now we set up a test model when the photons are placed in an inhomogeneous model,

4.5 Integrated flux in a narrowband filter

Until now we have shown the main effects of gas and dust rotation in the Ly α line morphology such as the escape fraction, the FWHM, the maxima position, also we see that shape of the outgoing spectra depends on the position of the observer. It is important to see if rotational effects are detectable in observational methods involving the Ly α line.

One of the most used methods to detect high redshift galaxies using the Ly α line is using a narrowband selection, we make this analysis based on the results obtained by Steidel (2011) in this work (EXPLAIN a bit more about their work) they used three narrowband filters for three different redshifts resumed in Table 2, We want to know how much the integrated flux change due to rotational effects in this NB filters, for the models we simulated with CLARA.

In table 2 we present the results of the flux in every narrowband filter for the homogeneous model at different velocities and hydrogen optical depth τ_0 . As is well known an increase in the optical depth makes the line peaks separation bigger. In fact for some cases the line width is larger than the NB filter width fig.(put ref fig) for those cases we modify the redshift in the available range in order to make the peak maxima match the NB filter center. For all cases we found that as velocity increase the flux is less.

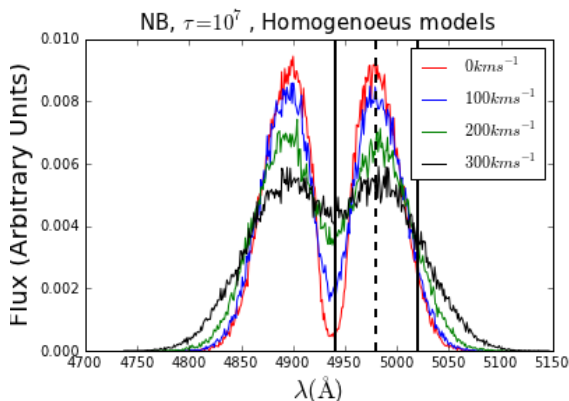
In the case of the dusty model we found the same trend of the flux with the velocity but in this cases the effect is not that strong. We also found some dependency with the viewing angle.

5 DISCUSSION

... Comparison with Verhamme et al. results on the rotation
... Compare with Kulas et al (Figure 3), Rotation on the Lyman alpha line convert double peak profiles into a single one. comments about rotation with inflows and outflows.

... The results derived in this paper have consequences on the interpretation of galaxy observations in the Lyman alpha line. ...compare steidel et al (2011)

Model	SSA22a 4980/80	HS1549 4667/80	HS1700 4018/90
V0HOM	0.99 / 0.90 / 0.40	1.0 / 0.96 / 0.52	1.0 / 0.99 / 0.66
V100HOM	0.94 / 0.81 / 0.40	0.98 / 0.90 / 0.51	0.99 / 0.96 / 0.64
V200HOM	0.74 / 0.74 / 0.40	0.81 / 0.81 / 0.48	0.87 / 0.87 / 0.59
V300HOM	0.59 / 0.59 / 0.39	0.66 / 0.66 / 0.45	0.73 / 0.73 / 0.54
V0HOMDust	0.99 / 0.99 / 0.93	0.99 / 0.99 / 0.86	0.99 / 0.99 / 0.92
V100HOMDust	0.99 / 0.98 / 0.91	0.98 / 0.96 / 0.86	0.99 / 0.98 / 0.9
V200HOMDust	0.91 / 0.90 / 0.86	0.83 / 0.81 / 0.72	0.88 / 0.87 / 0.81
V300HOMDust	0.83 / 0.82 / 0.79	0.67 / 0.66 / 0.61	0.74 / 0.74 / 0.70

Table 2. Values of fluxes for tree different NB and the our models simulated with CLARA**Figure 11.** NB filter located at the center of the maxima, with different redshift

6 CONCLUSIONS

In this paper we have estimated the effects of gas bulk rotation on the emission of the Lyman α line. We based the study on the study of a simplified configuration of an homogeneous sphere rotating as a solid body. We explored a range of models by varying the rotation speed, hydrogen optical depth, dust optical depth and initial distribution of Ly α photons with respect to the gas density. This was implemented in CLARA, a Monte-Carlo radiative transfer code already used to study the Lyman α line.

As first we see how the width of the line changes using a modified FWHM explained in section 4.1, and we found that as gas bulk rotation increase also the width increase in a factor of 2 – 3 in comparison with the static case. We also take into account the influence of the observer viewing angle, we found that observers with a line of sight perpendicular to the axis of rotation measure a 15% larger line width than those aligned with the rotation axis.

As many observational spectra Ly α emission line (Kulas et al) is double peaked, these peaks provide important information concerning gas kinematics and geometry, which can be partially explained with inflows/outflows of gas content. We study the effect of rotation in the position of this peaks, and we find that the position of the maxima does change with rotation for the homogeneous models when the double peak merged into a single peak as velocity increase. This effect is not seen for the central distribution when the double peak remains constant as the velocity increase. We also find that there is no dependency in the observer viewing angle with the maxima position.

Concerning the escape fraction under rotational effects on the Ly α emission line, we found that the escape fraction increase in about 20% – 30% for the homogeneous sphere model. While rotational effects are negligible for the central models and the escape fraction remains constant. Also the observer viewing angle have no effect in the escape fraction neither for the homogeneous and central models. Complementing this analysis we study the average number of scatterings $\langle N_{scatt} \rangle$ that photons perform before escaping of the cloud taking into account rotational effects. The main result here is for the homogeneous models for which as velocity increase photons escape with about $\sim 39\%$ less scatterings than in the static case.

As an application of these results we compute the integrated flux taking into account the narrow band filters used by (Steidel et al 2011), for our models we found an important decrease up to 40% for the homogeneous models, and up to 22% for the dusty homogeneous models in the flux as velocity increase. Also we calculate at what redshift should the filter be in order to get the maximum flux, and for the tree filters we get values that rely in the filter redshift range. This effects would have a relevant implication at the time to find high redshift galaxies.

This paper illustrates for the first time the main effects of rotation in the morphology of the Ly α emission line, we estimate the range of this effects for simplified models.

ACKNOWLEDGEMENTS

APPENDIX A: TABLES